AAS 13-334

LEVERAGING RESONANT ORBIT MANIFOLDS TO DESIGN TRANSFERS BETWEEN LIBRATION POINT ORBITS IN MULTI-BODY REGIMES

Mar Vaquero* **and Kathleen C. Howell†**

Resonant orbits have been widely employed in mission design for planetary flyby trajectories (JEO) and, more recently, as a source of long-term stability (IBEX). Yet, resonant orbits have not been explored extensively as transfer mechanisms between non-resonant orbits in multi-body systems. To highlight the benefit of employing resonant orbits for transfers and given the increased interest in employing libration point orbits for a variety of purposes, 2D and 3D transfers from LEO to the vicinity of the Earth-Moon libration points via resonant arcs are presented. Solutions are efficiently generated in the circular restricted three-body model and transitioned to a higher-fidelity model for validation. Direct optimization can further reduce the propellant requirements and a system translation technique is defined to add versatility to the proposed transfer design process, allowing for the quick translation of Earth-Moon transfers to other three-body systems.

INTRODUCTION AND MOTIVATION

Resonant orbits have been widely employed in mission design for multiple planetary flyby trajectories and, more recently, to support long-term stability. For instance, in support of a mission in NASA's Outer Planets Program, the Jupiter Europa Orbiter (JEO) spacecraft is designed to encounter two different resonances with Europa during the 'endgame' phase, leading to Europa orbit insertion on the final pass.[1–3] In 2008, the Interstellar Boundary EXplorer (IBEX) vehicle was launched into a high-altitude Earth orbit but, due to the strong and repeated perturbations from the Moon's gravitational field, the nominal mission trajectory became unpredictable in the long term. In 2011, the IBEX spacecraft was inserted into a remarkably stable out-of-plane lunar-resonant orbit, the first of this type for a spacecraft in a long-term Earth orbit.[4,5] However, resonant orbits have not yet been significantly explored as transfer mechanisms between non-resonant orbits in multi-body systems. It is well-known that Libration Point Orbits (LPOs) are fundamental structures in the mission design process; however, the dynamical environment in multi-body systems is not limited to LPOs. Thus, this investigation incorporates resonant orbits into the design process to potentially enable the construction of more efficient or even novel transfer scenarios. To explore such an option, it is necessary: 1) to expand the orbit architecture in the Earth-Moon (EM) Circular Restricted Three-Body Problem (CR3BP) by cataloging resonant orbits, and 2) to assess the role of resonant orbits in the design of transfer trajectories. Given the increased interest in employing Earth-Moon libration point orbits for a variety of purposes, transfer trajectories from a Low Earth Orbit (LEO) to

*Ph.D. Candidate, School of Aeronautics and Astronautics, Purdue University, Armstrong Hall, 701 West Stadium Avenue, West Lafayette, Indiana 47907-2045; Member AAS.

†Hsu Lo Professor of Aeronautical and Astronautical Engineering, School of Aeronautics and Astronautics, Purdue University, Armstrong Hall, 701 West Stadium Avenue, West Lafayette, Indiana 47907-2045. Fellow AIAA, AAS.

each of the five EM LPOs are designed by leveraging conic arcs and invariant manifolds associated with resonant orbits as well as libration point orbits. Resonant manifolds in the Earth-Moon system, particularly those emanating from exterior resonant orbits, offer trajectories that tour the entire Earth-Moon space in reasonable time intervals. These trajectories also pass relatively close to the Earth, offering good candidates for direct transfers from LEO. Then, the arrival phase into various LPOs is facilitated by the use of the associated LPO stable manifolds. Thus, the design technique that is employed to construct these efficient transfer trajectories exploits a variety of connecting arcs emerging from the manifolds associated with both resonant and libration point orbits. The CR3BP serves as a basis to quickly generate solutions that meet specific requirements. Candidate transfer trajectories are then transitioned to a higher-fidelity model that includes solar gravitational effects: 1) to validate the solutions generated in the 3B model, and 2) to demonstrate the existence of resonant conditions in multi-body regimes. A preliminary transfer cost and time-of-flight analysis illustrates the benefits of incorporating intermediate resonant arcs into the design process. To add versatility to the proposed transfer design method, an additional system translation technique is introduced to allow transfer trajectories in the EM system to be quickly translated to other systems.

MODEL FRAMEWORK

In any analysis involving resonance conditions, a resonance is typically defined initially within the context of the two-body problem and conics. However, this investigation is focused on resonance conditions involving multiple gravitational fields and, thus, the CR3BP serves as the basis for the problem formulation. In the restricted problem, the motion of an infinitesimal third particle, P_3, is modeled in the presence of two gravitationally-attracting bodies of significantly larger mass, P_1 and P_2. The motion of P_3 is governed by the well-known scalar, second-order differential equations of motion in standard form.[6,7] The state vector $\bar{X}$ is defined as the six-element state vector $[x\ y\ z\ \dot{x}\ \dot{y}\ \dot{z}]^T$, where the dot indicates a derivative with respect to the nondimensional time, τ, and relative to an observer in a rotating reference frame. The mass fraction μ is associated with the two system primaries P_1 and P_2, $\mu = \frac{m_2}{m_1+m_2}$, where m_1 and m_2 are the masses of P_1 and P_2, respectively. In this analysis, the value of the mass ratio in the Earth-Moon system is assumed to be $\mu \approx 0.0122$. The form of these equations of motion does admit an integral labeled the Jacobi constant, C, that is, $V^2 = 2U^* - C$, where the speed relative to the rotating frame is denoted V.

The existence of periodic motion in the CR3BP is well known and its computation in the nonlinear system involves the use of a multi-dimensional version of a Newton-Raphson differential corrections process implemented as a shooting method. With the availability of the appropriate mathematical model, that is, the equations of motion and the state transition matrix (STM), the nonlinear differential equations are numerically integrated to any future time. The STM is essentially a linear map reflecting variational behavior in the vicinity of a trajectory arc and predicts adjustments in the initial state to shift the final state to a desired set of values at the end point. Thus, this approximation is used to adjust the initial state such that the current trajectory evolves and reaches some desired state downstream; with the appropriate constraints, a periodic orbit is generated. An infinite number of periodic orbits exist in the CR3BP. Lyapunov and halo orbits are examples of planar and out-of-plane periodic motion near the libration points. Resonant orbits, by definition, are periodic as well but, in contrast to Lyapunov or halo orbits, are not typically associated with a particular Lagrange point.

RESONANT ORBIT ARCHITECTURE

Within the context of conics, a resonance exists when there is a simple numerical relationship between periods.[8] Orbit-orbit resonance is the focus of this investigation and is defined by the ratio *p*:*q*, where *p* is associated with the period of motion of the spacecraft and *q* reflects the period of the smaller primary, in this case, the Moon. In a multi-body problem, with the gravity of two or more bodies incorporated into the model, the ratio of the orbital periods is not rational, but rather an approximate rational fraction. In addition, the resulting orbits are not closed or periodic under these perturbations. A strategy is required to compute closed, periodic, resonant orbits in the CR3BP and a simple targeting scheme is applied. A first estimate for the initial state is generated from the two-body model. This starting vector seeds the corrections scheme to target a perpendicular crossing of the *x*-axis in a nonlinear propagation. Once a single, periodic, resonant orbit is determined, it is possible to generate multiple resonant orbits with the same characteristics, that is, a family of p:q resonant orbits, by employing a continuation scheme. Similar to families of libration point trajectories, such as Lyapunov orbits, planar families of resonant orbits also include bifurcating orbits that intersect families of 3D, periodic resonant trajectories. These bifurcating orbits are identified by examining the eigenvalues of the monodromy matrix corresponding to each orbit in the family and the presence of a bifurcating orbit is indicated by a change in stability. Once the bifurcating orbit is isolated, it is slightly perturbed in the z-direction and the resulting state seeds the corrections scheme to target a 3D resonant orbit. Representative members from a selection of planar (gray) and 3D (blue) families of symmetric *p*:*q* resonant orbits in the Earth-Moon system are plotted in Figure 1. Note that two bifurcating orbits exist in the planar family of 2:3 resonant orbits. Thus, two out-of-plane families of 2:3 resonant orbits are constructed and representative members are illustrated in Figure 1(e) and Figure 1(f).

The 3D families of orbits illustrated in Figure 1 represent out-of-plane resonant orbits, symmetric across the x-z plane, and are computed similarly to halo orbits, that is, by adding a small perturbation in the initial z-component. The initial state associated with any of these symmetric 3D resonant orbits has the form $\bar{x}_0 = [x_0 \;\; 0 \;\; z_0 \;\; 0 \;\; \dot{y}_0 \;\; 0]$. However, asymmetric 3D resonant orbits also exist and can be computed employing a similar corrections scheme. Such orbits are termed 'axial' resonant orbits and are calculated by slightly perturbing the bifurcating orbit in the $\dot{z}$-direction. The resulting initial state of the form $\bar{x}_0 = [x_0 \;\; 0 \;\; 0 \;\; 0 \;\; \dot{y}_0 \;\; \dot{z}_0]$ seeds the corrections scheme to target a 3D asymmetric resonant orbit by enforcing periodicity between the initial and final states. Representative members from a selection of 3D families of *p*:*q* 'axial' resonant orbits in the Earth-Moon system are plotted in blue in Figure 2. For reference, selected planar members are plotted in gray.

The restricted three-body model serves as a powerful tool to generate preliminary transfer trajectories in this analysis as it allows periodic orbits and invariant manifolds to be directly leveraged. However, to assess the impact of a higher-fidelity dynamical model, the CR3BP resonant orbits are transitioned to a dynamical model that incorporates n-body dynamics and planetary ephemerides. Note that periodic orbits in the CR3BP exist as quasi-periodic trajectories in a higher-fidelity model. To transition a CR3BP resonant orbit to an ephemeris model, each revolution along the orbit is first discretized into a series of patch points, which are then *stacked* to construct an orbit with a desired number of revolutions. A multiple-shooting algorithm yields a continuous trajectory in position and velocity in the full ephemeris model. To illustrate this transition process, a representative member from each resonant family is selected and using the trajectory in the CR3BP as the initial guess, the orbit is numerically generated in an Earth-Moon-Sun (EMS) point mass dynamical model incorporating the JPL DE405 ephemerides for the locations of the relevant bodies. The resulting 3D

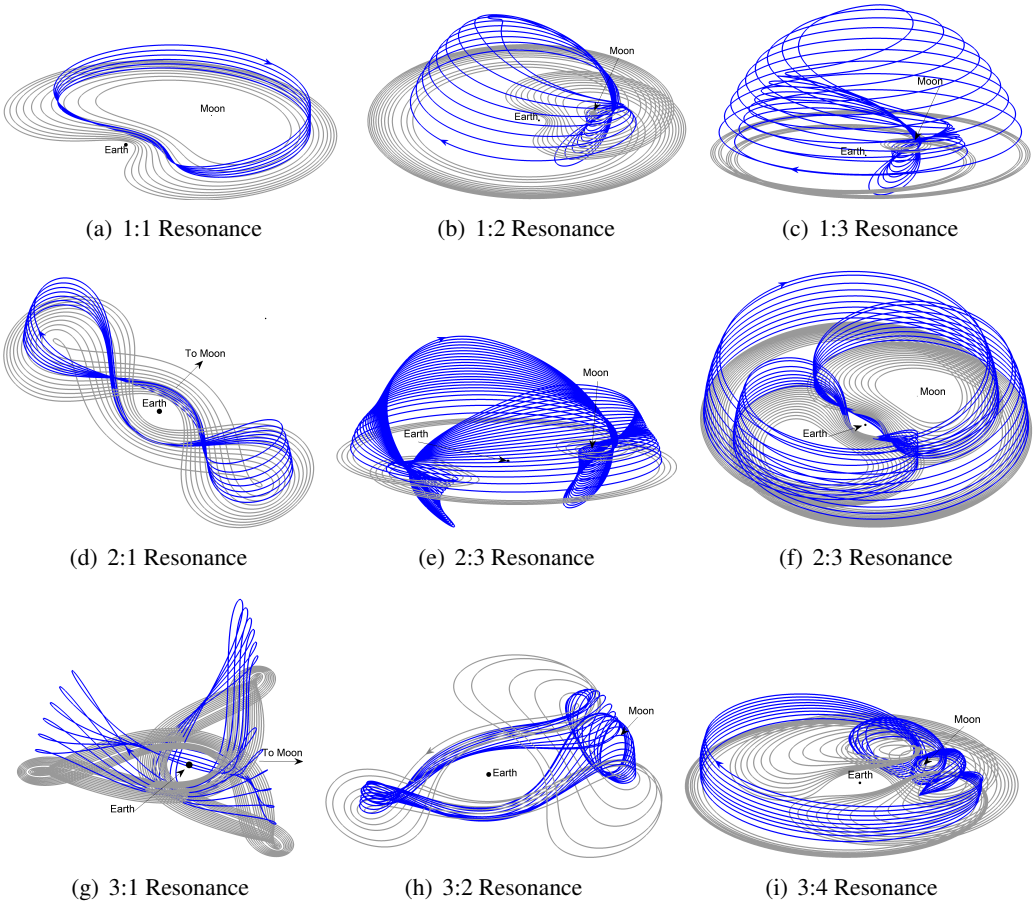

(a) 1:1 Resonance (b) 1:2 Resonance (c) 1:3 Resonance

(d) 2:1 Resonance (e) 2:3 Resonance (f) 2:3 Resonance

(g) 3:1 Resonance (h) 3:2 Resonance (i) 3:4 Resonance

Figure 1: Sample Orbits in 2D and 3D Families of p:q Resonant Orbits in the Earth-Moon System

quasi-periodic resonant orbits, plotted in purple, appear in Figure 3. For better visualization, only the planar projection is illustrated. Note that the period of these orbits and, thus, the resonant ratio, is preserved when transitioned to the full ephemeris model.

A particular class of resonant orbits in the Earth-Moon system has already proven quite useful in trajectory design for a specific mission scenario. The Interstellar Boundary Explorer (IBEX) spacecraft is currently located in a long-term stable Earth orbit and is also in resonance with the Moon's orbit. The selection of this particular orbit for the extended IBEX mission was based primarily on three factors: minimization of the radiation dose, improvement of science collection and avoidance of long eclipses.[4] Based on this criteria, the spacecraft was recently maneuvered from its nominal trajectory into this new stable orbit in a 3:1 resonance with the Moon. The extended orbit for the IBEX spacecraft resembles one of the 3D orbits plotted in Figure 1(g). This type of resonant orbit, along with other lunar resonant orbits, are likely useful for many types of mission trajectories, including weather and space science applications.[5] Note that, although the resonant families illustrated in Figures 1-3 are Earth-Moon periodic orbits, similar families of 3D resonant orbits are straightforwardly computed for different values of the mass fraction μ.[9,10] For instance, a family of planar 3:4 resonant orbits similar to the family that appears in Figure 1(i) is the focus of the Europa Orbiter end-game scenario.[2] Thus, resonant orbits are not only of interest from a dynamical analysis

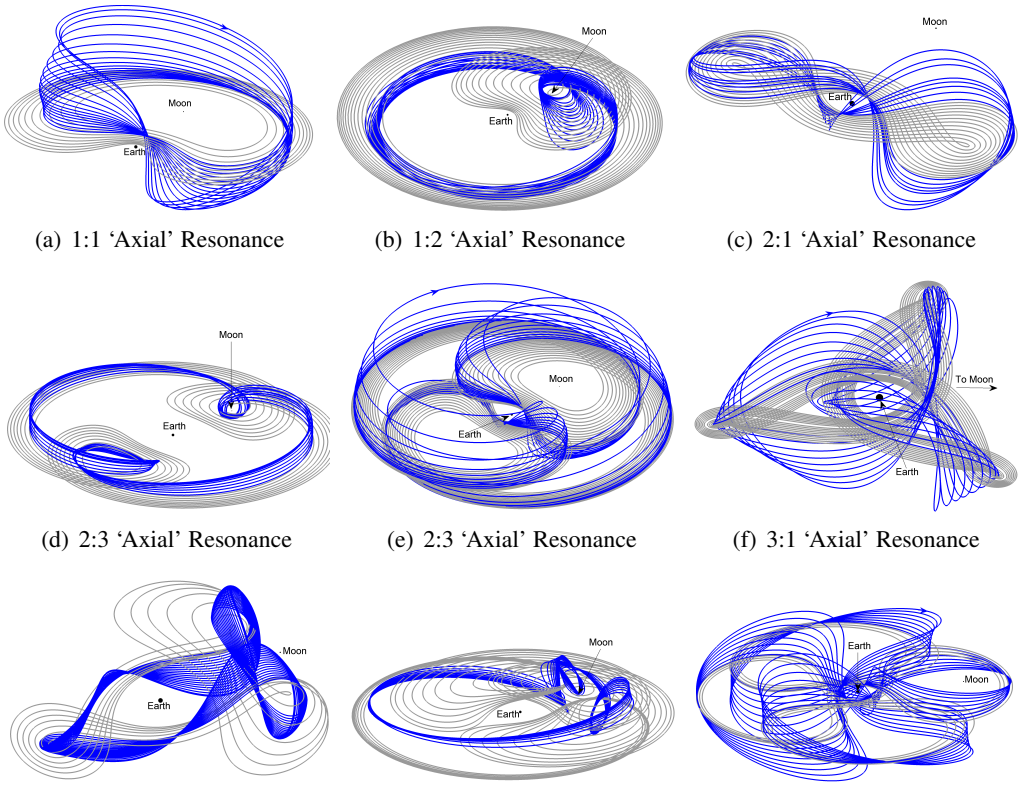

(a) 1:1 'Axial' Resonance (b) 1:2 'Axial' Resonance (c) 2:1 'Axial' Resonance

(d) 2:3 'Axial' Resonance (e) 2:3 'Axial' Resonance (f) 3:1 'Axial' Resonance

(g) 3:2 'Axial' Resonance (h) 3:4 'Axial' Resonance (i) 4:3 'Axial' Resonance

Figure 2: Sample Orbits in 3D Families of Axial Resonant Orbits in the Earth-Moon System

perspective but also for applications to meet current mission design requirements.

TRANSFER TRAJECTORY DESIGN STRATEGY

The role of invariant manifolds is significant in building a framework to model the dynamical environment in the CR3BP and, thus, knowledge of any manifold structure improves the efficiency of the trajectory design process in this regime. In contrast to the invariant manifolds associated with LPOs, the trajectories along the invariant manifolds corresponding to resonant orbits possess their own distinctive behavior.[2,3,11] However, the arcs are tangled, so plotting these paths in position space does not offer any clear insight. Thus, it is necessary to incorporate a technique that offers a different representation of these manifold trajectories. Maps that identify, and potentially isolate, the manifold trajectories aid in visualization and offer clues concerning the relationships between these manifolds and other structures in the phase space. A single map representation of these trajectories may not offer sufficient insight to construct efficient transfer trajectories between LEO and the LPO of interest. Therefore, three different mapping representations are employed in this analysis to identify the connecting arcs during the three phases that define a transfer between the initial LEO and the final resonant or libration point orbit. Consider a transfer from LEO to an Earth-Moon L_1 LPO. The various phases along a transfer path are identified in the diagram in Figure 4. The first phase links the LEO and the stable manifold arc associated with a resonant orbit. The second phase involves an arc that delivers the vehicle to the vicinity of the LPO of interest, and the third (and final) phase along the transfer trajectory is focused on the LPO insertion. Three different mappings,

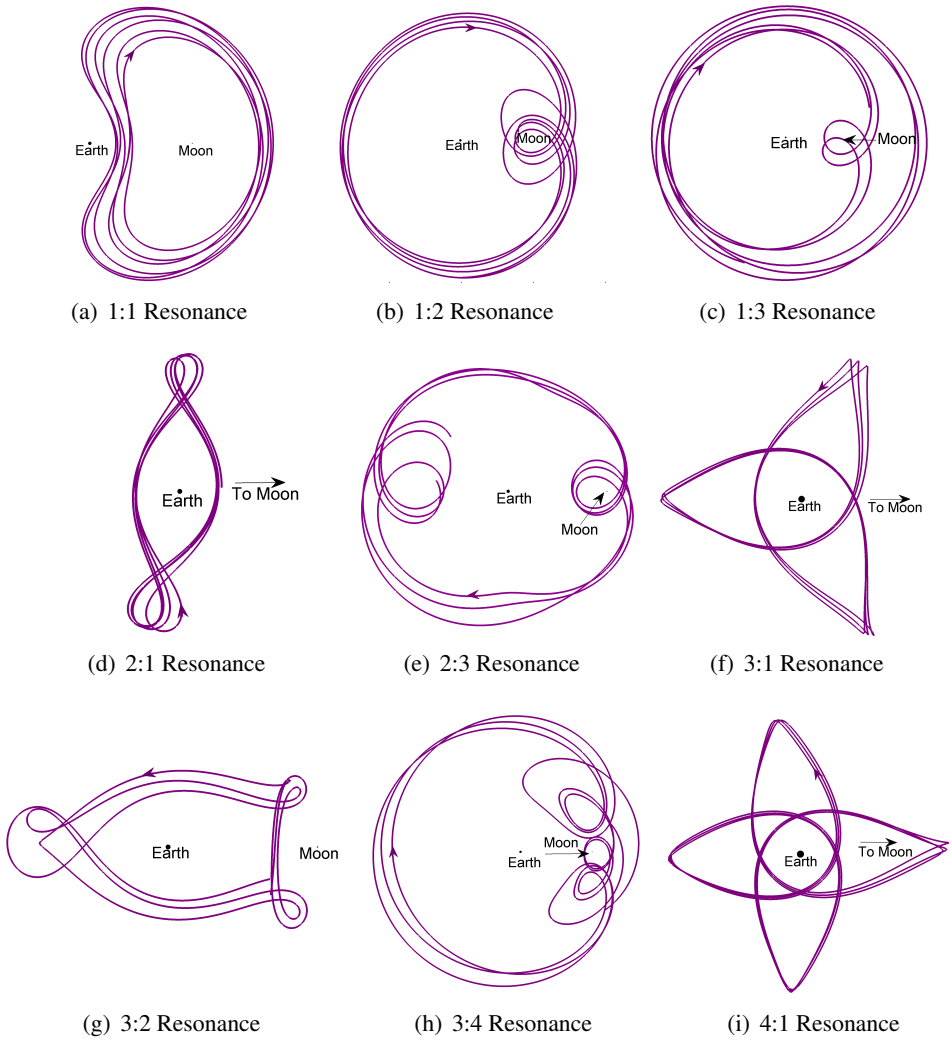

(a) 1:1 Resonance (b) 1:2 Resonance (c) 1:3 Resonance

(d) 2:1 Resonance (e) 2:3 Resonance (f) 3:1 Resonance

(g) 3:2 Resonance (h) 3:4 Resonance (i) 4:1 Resonance

Figure 3: xy-Views of Representative 3D Resonant Orbits in the Ephemeris Model

each associated with a transfer phase, supply a representation in a suitable design space: (i) a map reflecting position only (x-y) defined from apse locations,[12] and a position-velocity representation (x-$\dot{x}$ or y-$\dot{y}$) of the invariant manifolds on a surface of section defined at (ii) $y = 0$ and (iii) $x = K$, where K reflects a constant location along the x-axis, e.g., in the vicinity of the Moon, or $K = 1-\mu$. Once potential resonance transitions corresponding to each phase are identified from the maps, a corrections scheme is employed to blend the LEO, the connecting arcs and the arrival LPO into a continuous path. Although the resulting transfer paths benefit from a reduced maneuver cost (ΔV) by shadowing the manifold trajectories, direct optimization techniques are sometimes employed *a posteriori* to further reduce the propellant requirements. For reference, the strategy proposed in this analysis to construct transfer trajectories from LEO to the given EM libration point orbit as applied in this example is defined as follows:

- *Step 1.* Select and construct the arrival LPO as well as the resonant orbit that serves as the connection between the initial LEO and the final LPO

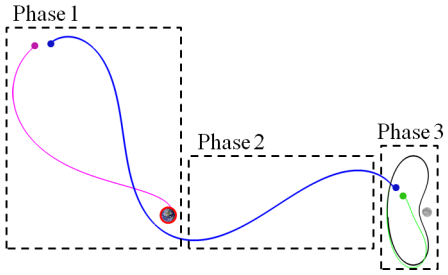

Figure 4: Transfer Phases Diagram

- *Step 2.* Generate a number of stable and unstable manifold trajectories associated with the selected resonant orbit and LPO by shifting off the periodic orbits in small steps in the direction of the stable and unstable eigenvectors, respectively.

- *Step 3.* Define the appropriate surface of section, i.e., $y = 0$, $x = K$, where K is a constant that defines a location on the x-axis near the smaller primary (e.g., $K = 0.65$) to generate the x-$\dot{x}$ and y-$\dot{y}$ maps, respectively. For this example, select $r\dot{r} = 0$ to construct the apse Poincaré map, where r is defined as the radial distance between the spacecraft and the Earth, i.e, $r = \sqrt{(x+\mu)^2 + y^2 + z^2}$, and $\dot{r}$ is the speed of the spacecraft relative to the rotating frame. Record the intersections of each manifold trajectory with the surfaces of section.

- *Step 4.* From the maps, identify potential transitions for each transfer phase and recover the appropriate intermediate arcs by integrating the states from a crossing on the map in forward time along the stable manifolds and backward time to produce the unstable manifolds. Recall that feasible connecting arcs are located from the intersection of stable and unstable manifolds on the maps. The arcs for Phase 1 are obtained from an intersection between the conic segments and the manifold trajectories. Likewise, the intermediate arcs for Phases 2 and 3 are identified from the intersection between manifold trajectories associated with resonant and libration point orbits.

- *Step 5.* Decompose the periodic orbits as well as the intermediate arcs into smaller segments and blend these subarcs into a trajectory that is continuous in position, allowing for intermediate ΔV maneuvers at specified patch points using a multiple shooting scheme. Design constraints, such as maximum ΔV or TOF, can be simultaneously applied to maintain the cost and the time-of-flight values within desired bounds.

- *Step 6.* One post-processing option includes the application of direct optimization techniques to the point solution to produce a locally optimal trajectory. The solutions in the three-body model can also be validated by transitioning the transfer path to a higher-fidelity model that includes planetary ephemerides and solar gravitational effects.

The maps are constructed only once after (i) the departure (LEO), arrival (LPO), and intermediate (resonant) orbits are selected, and, (ii) any associated manifolds are constructed. Thus, the transfer design process is straightforward and is easily automated to allow for the efficient construction of transfers with different patterns and itineraries.

APPLICATIONS IN THE EARTH-MOON SYSTEM

The effect of the Moon's gravity on periodic resonant orbits in the vicinity of the Earth can be significant, potentially delivering useful transfer scenarios. The large value of the mass parameter, μ, also influences the stability of the orbits in resonance with the Moon. Periodic resonant orbits in a family defined in terms of a p:q resonant ratio may be unstable in the Earth-Moon system but linearly stable in other systems. For instance, consider the family of 4:3 resonant orbits plotted in Figure 5. All members in the 4:3 resonant family in the Earth-Moon system are unstable; in contrast, most of the 4:3 resonant orbits in the Saturn-Titan family are linearly stable. The large gravitational effect of the Moon on resonant conditions reveals potentially useful transfer scenarios. In fact, the resonant orbits illustrated in Figure 5(a) offer a continuous "tour" of the system, and thus, these orbits are candidates for transfers to the vicinity of any of the five EM libration points. The periodic orbit plotted in Figure 5(c) is selected from the 4:3 EM family in Figure 5(a) to serve as a basis for the transfers that follow, but other members in the family can be employed, as well as other resonant orbits, to expand the design options.

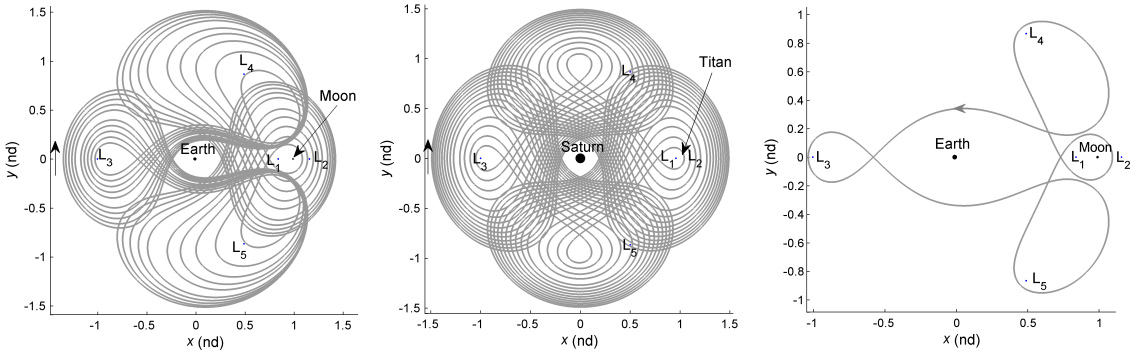

(a) Earth-Moon System (b) Saturn-Titan System (c) Selected 4:3 Resonant Orbit

Figure 5: Representative Members in a Family of 4:3 Resonant Orbits in the Earth-Moon and Saturn-Titan Systems in (a) and (b) and Selected EM Periodic Orbit for Transfers to LPOs in (c)

As an application of resonant orbits in the design of transfer trajectories to other, perhaps non-resonant, orbits in the Earth-Moon system, consider transfers from LEO to the vicinity of *any* of the libration points, L_i. Given the increased interest in utilizing Earth-Moon LPOs for different purposes, a variety of planar and 3D libration point orbits are considered in this preliminary transfer analysis. Sample orbits in the families of L_1, L_2, and L_3 Lyapunov orbits as well as sample short period orbits at L_4 and L_5 are represented in Figure 6(a). Likewise, representative members in the families of vertical and axial orbits at L_2, L_4 and L_5 are plotted in blue in Figures 6(b)-6(c), respectively. Sample LPOs in this transfer investigation are computed via a multiple shooting algorithm that incorporates a pseudo-arclength continuation scheme: families are constructed via a step in a direction tangent to the family.[13]

To construct the transfers, an initial 180-km altitude LEO and a final LPO are incorporated into the design process, as well as various intermediate segments. A total of two to three impulsive maneuvers are added along the transfer path. Recall that, in this analysis, a combination of conic arcs and invariant manifolds associated with resonant orbits as well as LPOs serve as the connecting segments. The manifolds are displayed on a surface of section to aid in the visualization of the trajectories in phase space and in locating regions of potential intersection that may yield low-

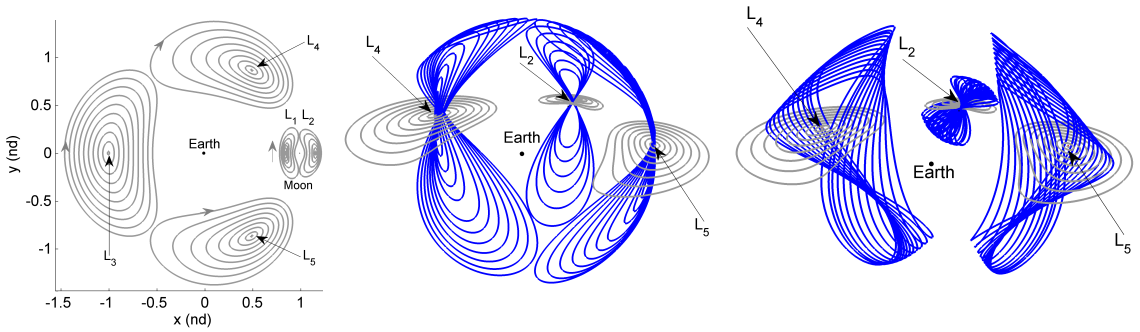

(a) 2D LPOs (b) 3D Vertical LPOs (c) 3D Axial LPOs

Figure 6: Representative Orbits in Families of 2D (Gray) and 3D (Blue) EM Libration Point Orbits

cost connections. A variety of mapping techniques are exploited to facilitate the design process and improve the connecting arcs that are selected as initial guesses for each transfer phase. The resulting Poincaré maps appear in Figure 7. The map in Figure 7(a) displays the apse locations of the stable manifolds associated with the resonant orbit (blue) as well as the conic segments (magenta) that serve as departure legs from LEO. For reference, representative LPOs are also plotted on the map. The maps in Figures 7(b)-7(c) offer a position-velocity representation of the conic arcs and the invariant manifold trajectories associated with the resonant orbit and the LPOs. The surfaces of section are located along the x-axis, i.e., $y = 0$, and at a given constant value, that is, $x = 0.65$, respectively. The resonant manifold trajectories (blue) in Figure 7(b) are also plotted against a background map (gray) that highlights other dynamical structures at this particular energy level and, thus, aids in the identification of regions of periodic, quasi-periodic, and chaotic motion in the vicinity of the Earth and the Moon. Recall that each Poincaré map is employed to identify a connecting arc for each phase along the transfer, that is, the apse map in Figure 7(a) is used for Phase 1 connecting an Earth departure leg (conic arc) to a stable manifold associated with a resonant orbit. The x-$\dot{x}$ map illustrated in Figure 7(b) highlights options for the intermediate – and longest – transfer arc for Phase 2, linking the vicinity of the Earth to the vicinity of the LPO of interest. Note that the segment in Phase 2 may be constructed from one or more intermediate arcs. Lastly, a path for the final approach to the LPO is obtained from the y-$\dot{y}$ map represented in Figure 7(c), exploiting manifold arcs emerging from both resonant orbits and LPOs. Note that only manifold trajectories are employed in the final transfer phase. Conic arcs serve as connecting legs between LEO and the intermediate manifold trajectories.

A selection of transfer trajectories that leverage conics as well as manifold arcs emerging from resonant orbits and libration point orbits are illustrated in Figures 8-10. The conic arc, or Earth departure leg, is represented in magenta, the stable manifold arc associated with the resonant orbit appears in blue, and the stable manifolds associated with the L_1 and L_2 LPOs are plotted in green. The arrival LPO is represented in black and the locations of the impulsive maneuvers that are required to construct a continuous transfer path from LEO to the selected EM LPO are highlighted in each plot. In all the sample transfers, the initial maneuver that is required to tangentially depart the 180-km LEO, i.e., ΔV_1, ranges in value between 3.10 km/s and 3.14 km/s. Note, however, that any initial altitude and inclination values can be easily incorporated into the transfer analysis, although

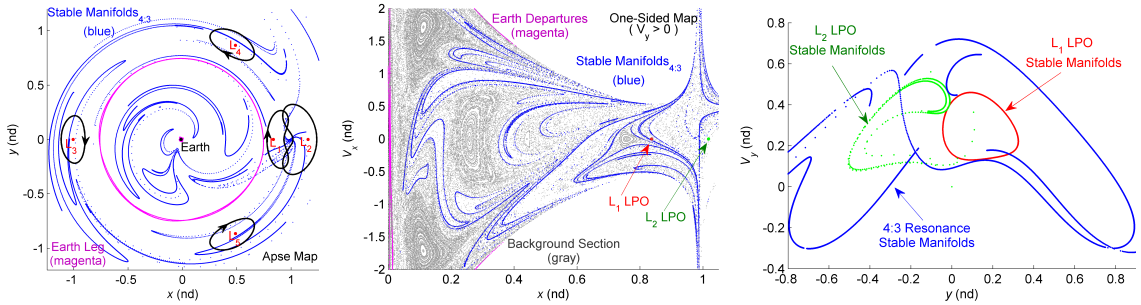

(a) Apse Map – Phase 1 (b) x-$\dot{x}$ Map ($y = 0$) – Phase 2 (c) y-$\dot{y}$ Map ($x = 0.65$) – Phase 3

Figure 7: Poincaré Maps Illustrating the Relationship between the Conic Arcs and Invariant Manifolds Associated with Resonant Orbits and LPOs for Each Transfer Phase

the initial cost of departure is influenced by the initial departure orbit. The cost associated with the remaining maneuvers, i.e., ΔV_2 and ΔV_3, as well as the time-of-flight (TOF), are detailed in Table 1 for each transfer. Note that the cost and time-of-flight associated with the L_1, L_2 and L_3 transfers is not optimized, although these transfers certainly benefit from a reduced ΔV-cost and TOF. For reference, the arcs that serve as initial guesses to generate the transfer paths are labeled on each figure.

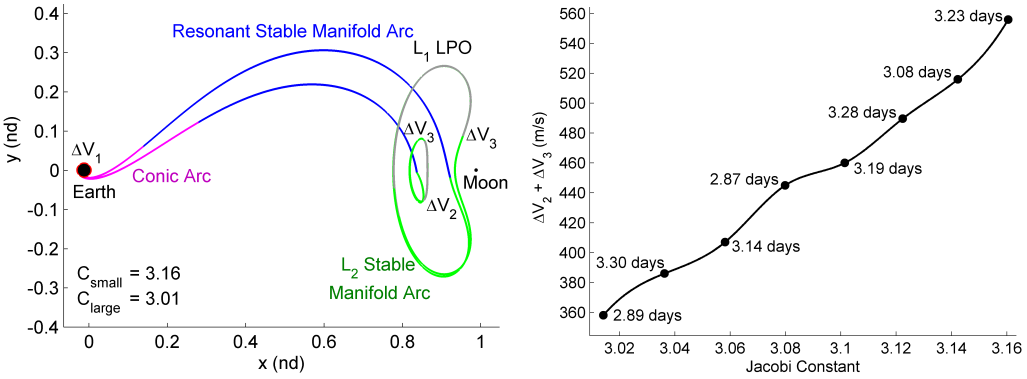

(a) LEO-L_1 Transfers ($C = 3.16$ and $C = 3.01$) (b) Cost and TOF Analysis

Figure 8: Transfers to Selected EM L_1 LPOs via Conic, Resonant and LPO Manifold Arcs in (a) and Maneuver Cost and Time-of-Flight As a Function of Jacobi Constant in (b)

Incorporating resonant manifold arcs into the transfer design process may supply alternative transfer scenarios or even reduce the cost associated with transfer trajectories to LPOs. However, an isolated transfer trajectory may not provide insight into the transfer options. To gain a better understanding of the effect of blending a combination of conic, resonant and LPO manifold segments, transfer trajectories to a range of L_1 and L_2 Lyapunov orbits at different energy levels are considered. The associated intermediate cost of the transfer to each arrival orbit is evaluated as a function of Jacobi constant and appears in Figures 8(b)-9(b). For reference, the associated time-of-flight is also labeled for each transfer trajectory. The general trend for the transfers to the vicinity of L_1 is expected: the maneuver cost increases as the value of Jacobi constant decreases, that is, it is more efficient to insert into larger y-amplitude Lyapunov orbits. Generally, the time-of-flight follows a

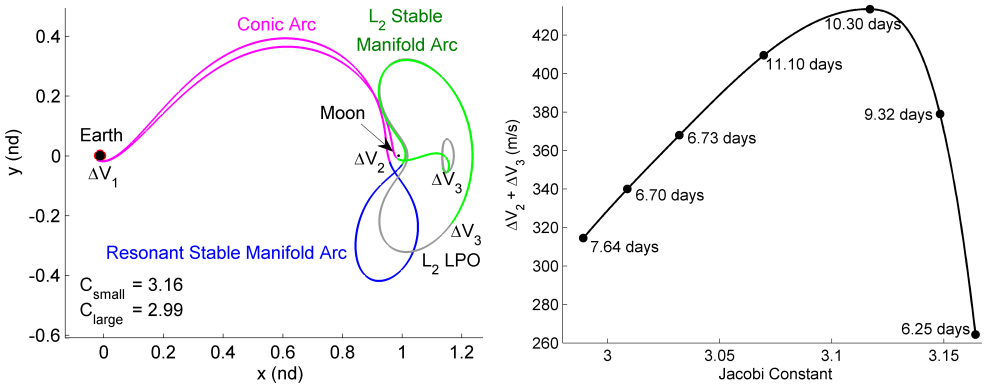

(a) LEO-L_2 Transfers ($C = 3.16$ and $C = 2.99$) (b) Cost and TOF Analysis

Figure 9: Transfers to Selected EM L_2 LPOs via Conic, Resonant and LPO Manifold Arcs in (a) and Maneuver Cost and Time-of-Flight As a Function of Jacobi Constant in (b)

similar pattern, that is, the transfer duration decreases as the value of Jacobi constant increases; in other words, it is faster to insert into larger y-amplitude Laypunov orbits at L_1. For transfers to the vicinity of L_2, the behavior is slightly different. It appears to be equally efficient to insert into both higher- and lower-energy Lyapunov orbits at L_2 in a global sense. As expected, it is more affordable to access higher-energy orbits at L_2. However, it is possible to insert into the lower-energy orbits by exploiting the gravitational effect of the Moon, that is, by introducing the intermediate maneuver, ΔV_2, in the vicinity of the Moon. The cost of inserting into the lowest-energy orbit in this preliminary transfer analysis is low and the time-of-flight is short, suggesting that more efficient options may be available even at lower energies. Recall that these transfer trajectories to the vicinity of L_1 and L_2 are sub-optimal trajectories and, thus, more cost effective options may be available.

A number of transfer trajectories from LEO to LPOs at L_3, L_4, and L_5 are generated using the same design approach. A sample of three trajectories appear in Figure 10, although other examples are available. In contrast to the periodic libration point orbits considered at L_2, the LPOs at L_3, L_4, and L_5 are linearly stable, that is, there is no natural flow to and from the orbit that can be exploited to access these orbits. Therefore, only a combination of conic segments and manifold arcs associated with resonant orbits are employed to construct the transfer trajectories in Figure 10. Note, however, that the maneuver cost to access L_3, L_4, and L_5 is generally lower than to insert into L_1 and L_2 LPOs, but the time-of-flight is inevitably longer. With the aid of the automated design process, the transfer arcs are combined to design a tour of all five selected LPOs. A return segment to Earth is added from the LPO at L_3. A total of six intermediate maneuvers are required to transition between these regions, i.e., $\Delta V_{2:7} = [374.12 \;\; 58.11 \;\; 49.21 \;\; 80.44 \;\; 79.41 \;\; 29.59]$ m/s and the time-of-flight between the LPOs is 165 days. An expectedly large initial maneuver is required to depart LEO, i.e., $\Delta V_1 = 3.13$ km/s, and a departure maneuver from the LPO at L_3 allows a return to LEO, i.e., $\Delta V_8 = 634.17$ m/s. Note that other tours with different itineraries can be also constructed.

Any transfer trajectory from Earth to the libration points constructed by linking stable and unstable manifold segments associated with resonant or libration point orbits is a sub-optimal trajectory, although it benefits from a reduced cost. However, it is possible to locally optimize these transfer trajectories. As an illustrative example, the transfer trajectory to the vicinity of L_5 from an initial 180-

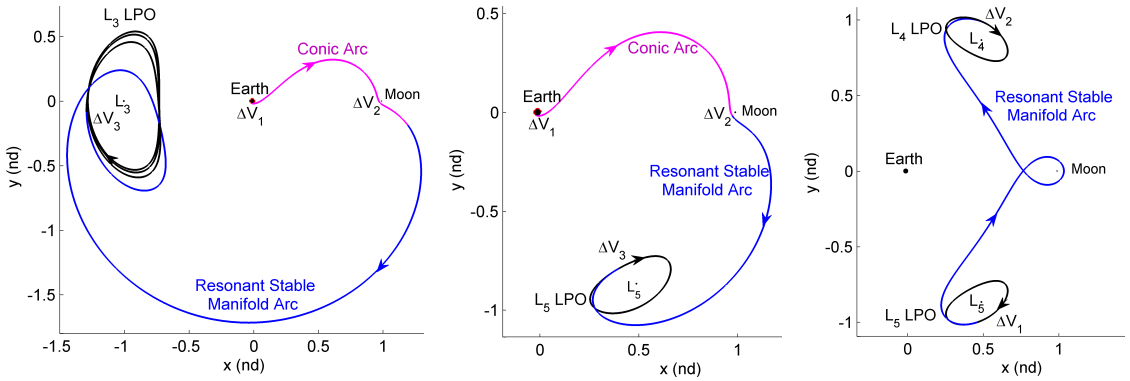

(a) 2D LEO-L_3 Transfer (b) 2D Optimal LEO-L_5 Transfer (c) 2D L_5-L_4 Transfer

Figure 10: Transfers to Selected EM L_3, L_4, and L_5 LPOs via Conic and Resonant Manifold Arcs

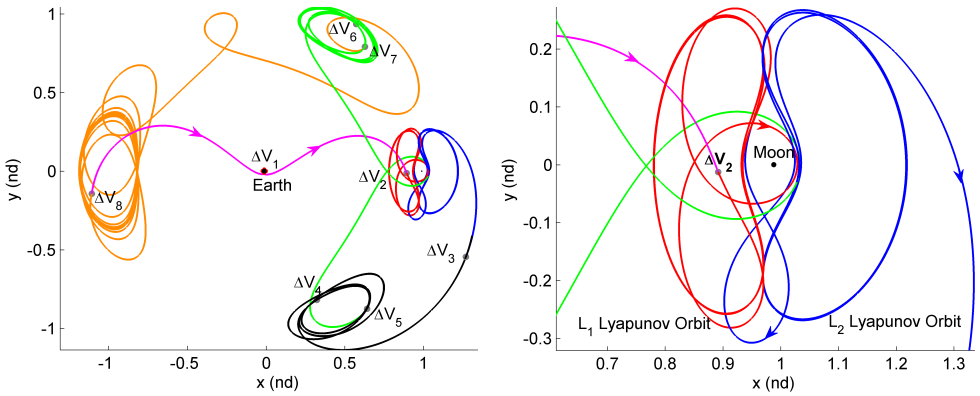

(a) Libration Point Orbit Tour (b) Zoomed-View of L_1 and L_2 Region

Figure 11: Tour of Five LPOs in the EM System with 180-km LEO Departure and Arrival

km LEO represented in Figure 10(b) is considered for optimization. In the optimization process, a single, locally optimal transfer trajectory is identified by 1) specifying the desired departure and arrival orbits and 2) modifying the initial velocity of the spacecraft along each of the intermediate connecting arcs as well as the time-of-flight associated with each segment. To add flexibility to the algorithm, the initial and final position states on the transfer trajectory are not fixed but are constrained to the departure and arrival orbits, which is achieved by varying the integration times along the periodic orbits and by formulating the initial and final position states as equality constraints. The decision variables include the initial position and initial velocity associated with the transfer arcs and the integration times, that is, $\bar{X} = [x_{0C}\ y_{0C}\ z_{0C}\ \dot{x}_{0C}\ \dot{y}_{0C}\ \dot{z}_{0C}\ x_{0R}\ y_{0R}\ z_{0R}\ \dot{x}_{0R}\ \dot{y}_{0R}\ \dot{z}_{0R}\ \mathrm{TOF_{LEO}}\ \mathrm{TOF_C}\ \mathrm{TOF_R}\ \mathrm{TOF_{L5}}]^{\mathrm{T}}$, where sub-vectors in $\bar{X}$, $\bar{X}_{0C}$ and $\bar{X}_{0R}$, represent the 6D initial states associated with the conic and resonant arcs, respectively. Recall that, because of the stability, manifolds associated with the selected libration point orbits are not available and, thus, only resonant manifold arcs are considered. The first ($\mathrm{TOF_{LEO}}$) and fourth ($\mathrm{TOF_R}$) integration times specify the departure and arrival locations along the LEO and along the short period orbit at L_5, respectively. The intermediate integration times, i.e., $\mathrm{TOF_C}$ and $\mathrm{TOF_R}$, correspond to the times of flight along the conic arc and the resonant manifold arc that link the initial and final orbits. The objective

function returns the magnitude of the minimum initial, intermediate, and final maneuvers that are required to depart the 180-km LEO orbit and to insert into the selected L_5 short period orbit, that is, $f(\bar{X}) = \Delta V_1 + \Delta V_2 + \Delta V_3$. A number of optimization algorithms can potentially be employed to solve the problem. One common and robust nonlinear programming algorithm is based on Sequential Quadratic Programming (SQP). The SQP routine is a quasi-Newton direct method of minimizing a continuous nonlinear objective function by solving a simpler quadratic programming sub-problem. The resulting optimal transfer trajectory is plotted in Figure 10(b) and the magnitude of the minimum initial, intermediate and final maneuvers along with the associated time-of-flight are detailed in Table 1. Note that, for brevity, the original sub-optimal transfer is not included, but the total transfer cost and the TOF are reduced by 260 m/s and 4 days, respectively. The optimization process is illustrated via this particular example, but all other transfers offer good candidates for further cost reduction as well. An alternative approach to reduce the propellant consumption is the incorporation of a maximum-ΔV_T constraint to the corrections algorithm, that is, to limit the magnitude of the total maneuver cost by specifying an upper bound: $\Delta V_T \leq \Delta V_{max}$. The resulting transfers are sub-optimal solutions, yet cost efficient.

The transfer design technique is not limited to the planar problem. Natural transfers between 3D resonant orbits as well 3D transfers from Earth orbit to out-of-plane resonant orbits exist and are calculated with the aid of higher-dimensional Poincaré maps.[14] Similarly, it is possible to generate 3D transfer trajectories to the vicinity of EM LPOs by exploiting 3D resonant and LPO manifold arcs via a modified corrections scheme. As an example, consider an out-of-plane transfer from LEO to a 3D axial orbit near L_4. In contrast to similar periodic orbits at L_1 and L_2, the selected axial orbit at L_4 is linearly stable, and thus, manifold trajectories to access the orbit are not available. Consequently, a maneuver is required to insert into the L_4 axial orbit. To construct the out-of-plane transfer, two periodic orbits are considered: a member from the family of 3:2 axial resonant orbits plotted in Figure 2(g) and a sample axial orbit at L_2 that is part of the family plotted in Figure 6(b). Then, a stable manifold trajectory associated with the axial orbit at L_2 offers a transition arc from the LEO to the vicinity of the Moon and an unstable manifold trajectory associated with the 3:2 axial resonant orbit supplies the path to the vinicity of L_4. Note that the use of a conic arc to connect the initial Earth orbit to the stable manifold is not necessary as the manifold trajectories associated with the axial orbit at L_2 pass close to the Earth. The initial and final orbits along with the intermediate arcs are blended using a corrections scheme and the resulting transfer trajectory appears in Figure 12. For reference, the stable and unstable manifolds are highlighted in green and red, respectively. A total of three impulsive maneuvers are incorporated throughout the transfer path; however, the cost associated with linking the two intermediate manifold arcs is reduced to zero. For completeness, the location of the maneuver is labeled in Figure 12. The largest plane change occurs in the vicinity of the Moon to significantly reduce the cost if insertion into the axial orbit at L_4 by leveraging the gravitational effect of the Moon. The associated cost of transfer and time-of-flight are detailed in Table 1. The selected orbit at L_4 is stable and the long-term stability is demonstrated by further propagating the end state of the transfer trajectory for 120 years. Consequently, little station-keeping is required to maintain the vehicle on the orbit over the long term. Other advantages associated with the selected orbit are full coverage of both the Earth and the Moon and uninterrupted communication capabilities. Therefore, given the small insertion maneuver and short time of flight, this transfer trajectory could be applicable in various design scenarios.

The versatility and potential usefulness of this design process is illustrated through various trajectory design scenarios but, ultimately, the solutions obtained in the CR3BP must be transitioned

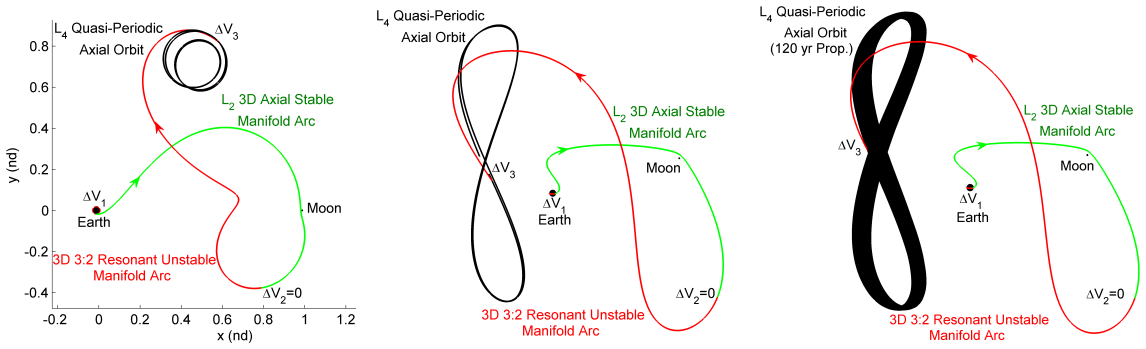

(a) xy-View (b) xyz-View (c) Long-Term Propagation

Figure 12: Transfer to Selected EM Axial Orbit at L_4 via Conic, Resonant and LPO Manifold Arcs

to higher-fidelity models for validation. To illustrate the impact of additional gravitational forces on the solutions initially generated in a 3B model, the optimal transfer trajectory from LEO to the vicinity of L_5 in Figure 10(b) is generated in an ephemeris model including solar gravity effects. Recall that periodic orbits in the CR3BP exist as quasi-periodic trajectories in the ephemeris model. Therefore, the design constraint that enforces the end state along the transfer path to occur along the specified periodic arrival orbit is no longer applicable in the full model. Alternatively, arrival to a quasi-periodic orbit is enforced. The resulting path in the ephemeris model appears in purple in Figure 13(a); the relationship between the CR3BP and the ephemeris transfer trajectory is apparent and the associated total maneuver cost is similar. However, the cost associated with the trajectory in the full model is dependent on the epoch, that is, departure during certain months of the selected year (2020) are more cost effective than others. To address this dependency, a preliminary cost analysis appears in Figure 13(b), illustrating the transfer cost as a function of the initial epoch. For reference, the transfer cost associated with the CR3BP transfer is also labeled on the plot. In general, launching during the summer months is less cost effective than during the winter months. Note that the ephemeris trajectories are not optimal and, thus, more efficient solutions may be available.

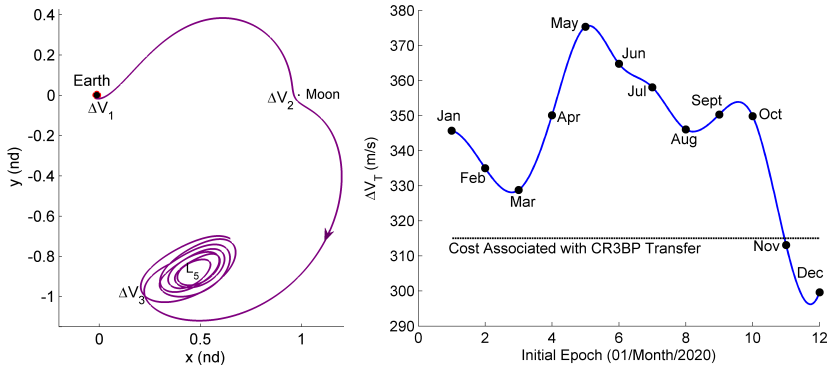

(a) LEO-L_5 Ephemeris Transfer (b) Preliminary Cost Analysis

Figure 13: Transfer to Short Period Orbit at L_5 in the Ephemeris Model in (a) and Cost Chart in (b)

The cost and time-of-flight associated with the selected transfer trajectories from LEO to the EM

Table 1: Maneuver Cost and Time-of-Flight Associated with Transfers in Figures 8-13

Figure	Transfer	ΔV_1 (km/s)	ΔV_2 (m/s)	ΔV_3 (m/s)	ΔV_T (km/s)	TOF (Days)
8(a) (small)	LEO - L_1	3.12	555.00	0.80	3.67	3.23
8(a) (large)	LEO - L_1	3.13	358.00	0.80	3.46	2.89
9(a) (small)	LEO - L_2	3.13	264.40	0.75	3.39	6.25
9(a) (large)	LEO - L_2	3.12	314.15	1.00	3.43	7.64
10(a)	LEO - L_3	3.10	166.96	33.03	3.30	31.74
12(c)	LEO - L_4 Axial	3.10	170.00	0.00	3.27	22.54
10(c)	L_5 - L_4	–	77.03	72.96	0.15	26.67
10(b)	LEO - L_5 (EM)	3.10	261.84	39.24	3.40	23.78
13(a)	LEO - L_5 (EMS)	3.10	226.56	33.43	3.36	23.78

LPOs are very reasonable and comparable to Earth-Moon transfer trajectories available in the literature,[15–17] including transfers to libration point orbits[18,19] that exclusively exploit invariant manifolds associated with LPOs. Thus, the addition of resonant orbits to the transfer design process may offer more insight into the design space and potentially deliver more efficient transfer trajectories. Note also that departure and arrival along the periodic orbit is enforced in all of the CR3BP transfers. However, the transfer cost can be significantly reduced – in some cases by over 100 m/s – if this design constraint is relaxed, i.e., if the arrival orbit is allowed to be slightly quasi-periodic. Nevertheless, the goal in this analysis is not to produce minimum-ΔV or TOF transfer trajectories but (i) to supply quick and efficient maps for the generation of candidate transfers, and (ii) to demonstrate the applicability of resonant orbits as transfer mechanisms between non-resonant orbits in multi-body environments. The Earth-Moon space is selected for exploration since the gravitational influence of the Moon on resonant orbits reveals a variety of resonant families and transfer design scenarios, but the design technique is applicable to other multi-body systems.

THREE-BODY SYSTEM TRANSLATION

Transfer trajectories with predetermined itineraries are efficiently generated exploiting dynamical structures and Poincaré mapping techniques. However, orbital characteristics vary from system to system and a number of computations are required before the desired transfer trajectory is produced. The capability of selecting a trajectory in the Earth-Moon system and directly translating it to a different three-body system without the necessity of generating periodic orbits, invariant manifolds, and Poincaré maps in the new system is valuable. Thus, a system translation technique is detailed to generate sample transfers in the Saturn-Titan and Saturn-Enceledus systems directly from transfers in the Earth-Moon system.

Earth-Moon System to Saturn-Titan System

Different strategies are available to translate a point solution from one 3B system to another, but perhaps the simplest approach is the use of a multiple shooting algorithm wrapped in a single-parameter continuation scheme, where the mass parameter, μ, is progressively varied until the desired value is achieved. This corrections scheme is implemented in a particularly straightforward manner when the point solution to be translated from one 3B system to another is a periodic, resonant orbit. As an illustrative example, consider a sample 3D 3:1 axial resonant orbit from the family

represented in Figure 2(f). The periodic orbit in the Earth-Moon system serves as the initial guess that seeds the differential corrections algorithm. Then, the mass parameter associated with the converged solution, i.e., μ_{EM}, is varied. Employing the successful orbit with the perturbed parameter as a new guess, the differential corrections algorithm produces a second converged solution, that is, a new periodic, resonant orbit in a system with a different mass parameter. This process is continued until the desired value of the mass parameter (μ_{ST}) is achieved and a converged solution in the Saturn-Titan system is produced. The resulting resonant orbit in the Saturn-Titan system is illustrated in Figure 14. For reference, the original axial resonant orbit in the Earth-Moon system is also plotted in blue. Note, however, that the primaries depicted in Figure 14 are Saturn and Titan and the nondimensional units are scaled differently in each system ($l^*_{EM} = 384400$ km and $l^*_{ST} = 1221830$ km). Consequently, the size of the orbits differ but the general characteristics are preserved. The similarities between the two orbits are apparent but the computation process is remarkably faster for the orbit in the Saturn-Titan system since no *a priori* knowledge of the design space is necessary to generate the orbit. To demonstrate the validity of the translated solution, the Saturn-Titan orbit is integrated in a higher-fidelity model. The initial epoch is randomly selected to be June 1, 2020 and a total of 10 revolutions are stacked to create the ephemeris orbit represented in Figure 14(c).

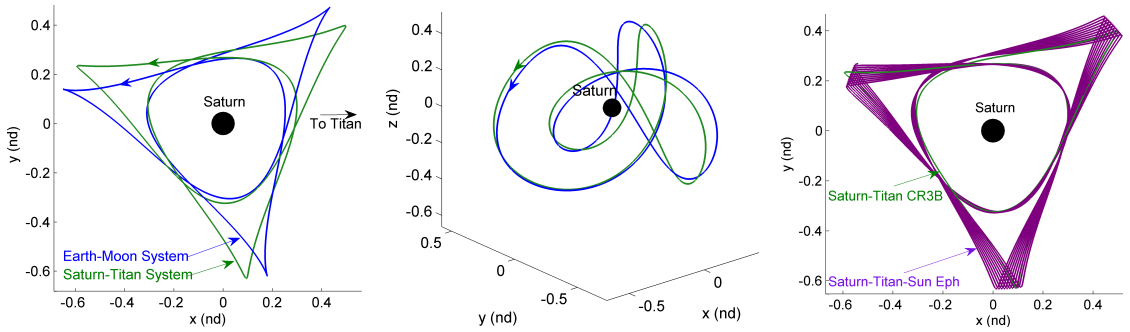

(a) (b) (c)

Figure 14: 3:1 Axial Resonant Orbit in Earth-Moon System (Blue), Saturn-Titan System (Green), and Ephemeris Model (Purple) Computed via System Translation Technique

The translation of transfer trajectories to different systems does offer challenges; for example, the proximity of the trajectory to Earth at departure and the low perilune altitude may result in convergence difficulties when the mass parameter is varied. To avoid convergence issues, additional constraints are enforced along the transfer path. Before initializing the mass parameter continuation scheme, the size of the departure orbit is increased to accommodate the size difference between the two larger primaries in each system, that is, the Earth and Saturn. A single-parameter continuation scheme is implemented to shift the initial 180-km LEO to a Saturn-centered circular orbit with altitude $h = 0.2$ nondimensional units, equivalent to 244,366 km. For reference, the E Ring, Saturn's second outermost ring, is located at 166,000 km from the surface,[8] originating near the orbit of Mimas and terminating near the orbit of Rhea. To avoid impact with the smaller primary, a minimum closest approach distance constraint is also implemented. Once the additional constraints are enforced, the mass parameter continuation process is initialized. To illustrate the process, consider the transfer trajectory to the quasi-periodic axial orbit at L_4 represented in Figures 12(a)-12(b). The 3B system translation technique is applied to the original EM transfer and the resulting trajectory in the Saturn-Titan system is plotted in Figure 15. The intermediate arcs differ slightly, but the axial orbit

at L_4 preserves its general characteristics. To add further flexibility to the algorithm, the inclination of the departure orbit is allowed to vary, that is, the position of the first patch point is constrained to be on a sphere of radius $r = 0.2$ nondimensional units. For illustration purposes, the departure sphere is illustrated as a gray sphere centered at Saturn.

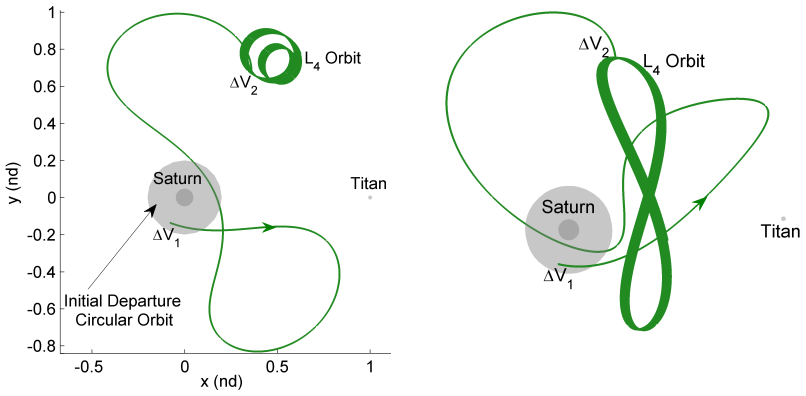

(a) xy-View (b) xyz-View

Figure 15: Transfer to a Quasi-Periodic Axial Orbit at L_4 in the Saturn-Titan System After Translation from a Similar Earth-Moon Trajectory

The main advantage offered by the system translation technique is that no *a priori* knowledge concerning the design space is required to construct a transfer in a different 3B system, resulting in a fast and efficient method of generating preliminary trajectories. Initially, a continuous path is sought when translating a solution from the Earth-Moon system to the Saturn-Titan system. However, additional design constraints can be incorporated to produce a transfer path with a specific pattern. For example, if desired, a flyby altitude at Titan can be specified and the propellant consumption and time-of-flight can be constrained after a continuous path is produced.

Earth-Moon System to Saturn-Enceladus System

Saturn's tiny icy moon Enceladus is a popular solar system destination for future robotic missions, but the insignificant size of Enceladus and its close proximity to Saturn combine to render a challenge in the design of transfer trajectories in such a multi-body environment. Nevertheless, the mass parameter continuation scheme is employed to translate point solutions directly from the Earth-Moon system to the Saturn-Enceladus system. For reference, the mass parameter in the Saturn-Enceladus system is five orders of magnitude smaller than the mass parameter in the Earth-Moon system, that is, $\mu_{SEnc} = 1.9 \times 10^{-7}$. The almost negligible gravitational effect of Enceladus on the spacecraft path not only complicates the design process but reduces the availability of natural trajectories. Most resonant orbits in the Saturn-Enceladus system are linearly stable, but even for the few unstable orbits, the manifold trajectories are bounded in the exterior region near the zero velocity curves. Thus, there is limited availability of manifold trajectories that travel to the vicinity of Saturn. Hence, a preliminary transfer from a Saturn-centered circular orbit to a libration point orbit via a manifold-based approach is a particular challenge. However, the mass parameter continuation scheme offers an alternative transfer construction process initiated from a previously known trajectory with specific characteristics in the Earth-Moon system.

Distant retrograde orbits (DROs) generally exhibit long-term stability and are of particular interest for a variety of missions.[20] Hénon, who initially examined DROs, labeled them the 'f family'.[21] Although most members in a family of DROs are linearly stable, there is a small range of unstable DROs that pass near the larger primary, including an impact on the surface. The stability and the period associated with planar DROs are evaluated as a function of y-amplitude. For reference, unstable DROs appear in red and stable orbits are plotted in black in Figure 16(a). As illustrated in Figure 16(b), smaller y-amplitude DROs posses short periods (11 hrs) but the integration time along each orbit progressively increases until it reaches a plateau at $P = P_{Moon}$, i.e., approximately 27 days. Thus, part of the planar family is in a 1:1 resonance with the Moon. Additionally, the change in stability across family members indicates the presence of a bifurcation, from which a family of 3D DROs is generated. Representative members in the 3D family appear in Fig. 17(a). Note that out-of-plane DROs are in a 1:1 resonance with the Moon.

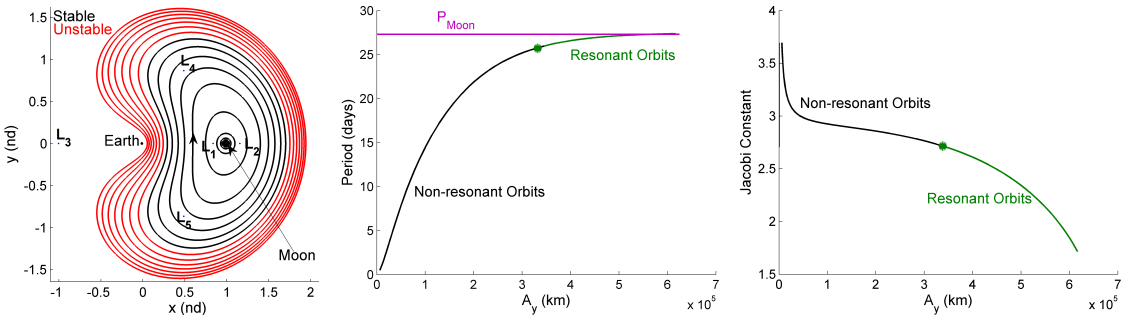

(a) Stable vs. Unstable DROs (b) Period vs. y-Amplitude (c) Energy vs. y-Amplitude

Figure 16: Stability, Energy, and Period Analysis of Planar DROs in the Earth-Moon System

Distant retrograde orbits have been investigated by numerous authors in different planar three-body systems. For instance, Lam and Whiffen explore the application of DROs around Europa.[20] Parker and Lo examine a family of DROs in the Earth-Moon system and their application in mission design[22] and Demeyer and Gurfil develop transfer trajectories from Earth to DROs in the Sun-Earth planar CR3BP.[23] To expand upon this application, a transfer from LEO to a 3D DRO in a 1:1 resonance with the Moon is constructed; the versatility of the proposed system translation technique is demonstrated by translating the EM transfer path to the Saturn-Enceladus system. The 3D DRO in a 1:1 resonance with the Moon, plotted in red in Figure 17(a), is selected as the arrival periodic orbit. A conic arc and a stable manifold trajectory associated with the 4:3 resonant orbit plotted in Figure 5(c) are combined to construct a transfer arc from a 180-km LEO to the selected DRO but no specific arrival location along the path is required. A multiple shooting algorithm with a number of design constraints is employed to generate the transfer trajectory plotted in Figure 17(b). Recall that the end state along the transfer path is constrained to be along the DRO. The mass parameter continuation scheme is then employed to generate a transfer trajectory with similar characteristics in the Saturn-Enceladus system. To simplify the algorithm, the constraint to arrive along the periodic orbit is removed and an alternative arrival at a 5-revolution quasi-periodic DRO is enforced. Otherwise, a new periodic DRO must be computed for each of the selected μ values throughout the mass parameter continuation process. The initial inclined departure orbit, plotted as a gray sphere in Figure 17(c), is also modified to be defined with an altitude of $h = 0.28$ nondimensional units.

The objective of the system translation process is not the immediate design of an optimal transfer

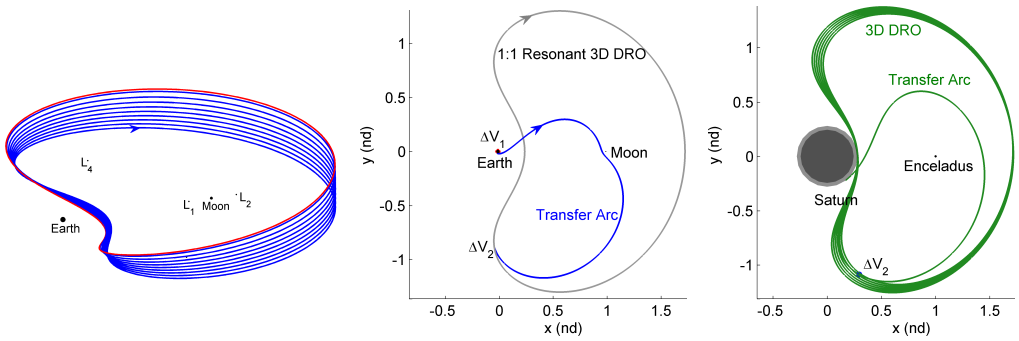

(a) EM 3D Resonant DROs (b) Earth-Moon Transfer (c) Saturn-Enceladus Transfer

Figure 17: Earth-Moon 3D Resonant DROs in (a), xy-View of a 3D Transfer to an EM DRO in (b), and xy-View of a 3D Transfer to a Quasi-Periodic DRO in the Saturn-Enceladus System in (c)

from a primary-centered circular orbit to a 3D DRO in either 3B system, but it is worth highlighting the maneuver cost and TOF associated with each transfer trajectory. In the Earth-Moon system, $\Delta V_2 = 228$ m/s and TOF $= 14.3$ days; in the Saturn-Enceladus system, the size of the maneuver is larger, i.e., $\Delta V_2 = 374.7$ m/s, but the time-of-flight is much shorter, i.e., TOF $= 0.93$ days. Optimization techniques can be applied *a posteriori* to further reduce the propellant requirements, time-of-flight or enforce other physical constraints along the transfer path.

SUMMARY AND CONCLUSIONS

An investigation of the dynamic environment correlated with 2D and 3D periodic resonant orbits within the context of the CR3BP is presented. Families of resonant orbits are a valuable addition to an existing map of the orbit architecture in the Earth-Moon system, potentially delivering useful trajectory design scenarios. The availability of reduced cost transfer trajectories is enabled through the exploitation of a combination of conic arcs and the invariant manifolds associated with resonant orbits and a variety of libration point orbits. Due to the complexity of the manifold structure emanating from resonant orbits, Poincaré maps are employed as an alternative visualization technique. From three particular mapping representations, appropriate intermediate segments are identified and employed as the initial guess for the construction of transfer trajectories with a wide variety of desired itineraries. Then, a robust and versatile corrections process yields a transfer path that meets the specified design constraints. Sample 2D and 3D transfer trajectories to a variety of Earth-Moon libration point orbits demonstrate the versatility of resonant orbits in trajectory design scenarios. Direct optimization is applied to reduce the maneuver cost and selected transfer solutions are transitioned to an ephemeris model for validation. To add versatility to the proposed design method, a 3B system translation technique based on a mass parameter continuation scheme is applied for the direct transition of Earth-Moon trajectories to the Saturn-Titan and Saturn-Enceladus systems.

ACKNOWLEDGMENT

The authors wish to thank Dr. Donald Dichmann at NASA Goddard Space Flight Center for valuable discussions on the computation of axial resonant orbits and their application to mission design. The authors appreciate the financial support from the School of Languages and Cultures and the School of Aeronautics and Astronautics at Purdue University as well as Zonta International.

REFERENCES

[1] NASA, "Planetary Science Decadal Survey: Jupiter Europa Orbiter Component of EJSM," March 2010.

[2] M. W. Lo, R. L. Anderson, G. Whiffen, and L. Romans, "The Role of Invariant Manifolds in Low Thrust Trajectory Design (Part I)," *AAS/AIAA Spaceflight Dynamics Conference*, Maui, Hawaii, February 2004. Paper AAS 04-288.

[3] R. L. Anderson and M. W. Lo, "The Role of Invariant Manifolds in Low Thrust Trajectory Design (Part II)," *AAS/AIAA Spaceflight Dynamics Conference*, Providence, Rhode Island, August 2004. Paper AIAA 2004-5305.

[4] J. Carrico et al., "Lunar-Resonant Trajectory Design for the Interstellar Boundary Explorer (IBEX) Extended Mission," *AAS/AIAA Astrodynamics Specialist Conference*, Girdwood, Alaska, July 31 - August 4 2011. Paper AAS-11-454.

[5] D. J. McComas et al., "A New Class of Long-Term Stable Lunar Resonance Orbits: Space Weather Applications and the Interstellar Boundary Explorer," *Space Weather*, Vol. 9, November 2011, p. 9.

[6] V. Szebehely, *Theory of Orbits: The Restricted Problem of Three Bodies*. New York, New York: Academic Press, Inc., 1967.

[7] M. Vaquero, "Poincaré Sections and Resonant Orbits in the Restricted Three-Body Problem," M.S. Thesis, School of Aeronautics and Astronautics, Purdue University, West Lafayette, Indiana, 2010.

[8] C. D. Murray and S. F. Dermott, *Solar System Dynamics*. Cambridge, United Kingdom: Cambridge University Press, Cambridge, 1999.

[9] M. Vaquero and K. C. Howell, "Poincaré Maps and Resonant Orbits in the Circular Restricted Three-Body Problem," *AAS/AIAA Astrodynamics Specialist Conference*, Girdwood, Alaska, July 31 - August 4 2011. Paper AAS-11-428.

[10] M. Vaquero and K. C. Howell, "Transfer Design Exploiting Resonant Orbits and Manifolds in the Saturn-Titan System," *Journal of Spacecraft and Rockets*. (In press).

[11] M. W. Lo, R. L. Anderson, T. Lam, and G. Whiffen, "The Role of Invariant Manifolds in Low Thrust Trajectory Design (Part III)," *AAS/AIAA Spaceflight Dynamics Conference*, Tampa, Florida, January 2006. Paper AAS 06-190.

[12] K. C. Howell, D. C. Davis, and A. F. Haapala, "Application of Periapse Maps for the Design of Trajectories Near the Smaller Primary in Multi-Body Regimes," *Mathematical Problems in Engineering*, Vol. 2012. Article ID 351759, 22 pages, 2012. doi:10.1155/2012/351759.

[13] E. J. Doedel et al., "Elemental Periodic Orbits Associated with the Libration Points in the Circular Restricted 3-Body Problem," *International Journal of Bifurcation and Chaos*, Vol. 17, January 2007, pp. 2625–2677.

[14] M. Vaquero and K. C. Howell, "Design of Transfer Trajectories Between Resonant Orbits in the Restricted Problem with Application to the Earth-Moon System," *1st IAA Conference on Dynamics and Control of Space Systems*, Porto, Portugal, March 19-21 2012. Paper IAA-AAS-DyCoSS1-05-09.

[15] E. Perozzi and A. Di Salvo, "Novel Spaceways for Reaching the Moon: An Assessment for Exploration," *Celestial Mechanics and Dynamical Astronomy*, Vol. 102, No. 1-3, 2008, pp. 207–218.

[16] K. E. Davis, G. H. Born, M. Deilami, A. Larsen, and E. A. Butcher, "Transfers to Earth-Moon L_3 Halo Orbits," *AIAA/AAS Astrodynamics Specialist Conference*, Minneapolis, Minnesota, August 13-16 2012. Paper AIAA 2012-4593.

[17] A. Larsen et al., "Optimal Transfers with Guidance to the Earth-Moon L_1 and L_3 Libration Points using Invariant Manifolds: A Preliminary Study," *AIAA/AAS Astrodynamics Specialist Conference*, Minneapolis, Minnesota, August 13-16 2012. Paper AIAA 2012-4667.

[18] J. S. Parker and G. H. Born, "Direct Lunar Halo Orbit Transfers," *AAS/AIAA Space Flight Mechanics Meeting*, Sedona, Arizona, January 28 - February 1 2007. Paper AAS-07-229.

[19] R. L. Anderson and J. S. Parker, "Comparison of Low-Energy Lunar Transfer Trajectories to Invariant Manifolds," *AAS/AIAA Astrodynamics Specialist Conference*, Girdwood, Alaska, July 31 - August 4 2011. Paper AAS-11-423.

[20] T. Lam and G. J. Whiffen, "Exploration of Distant Retrograde Orbits Around Europa," *15th AAS/AIAA Spaceflight Mechanics Meeting*, Copper Mountain, Colorado, January 23-27 2005. Paper AAS-05-110.

[21] M. Hénon, "Numerical Exploration of the Restricted Problem. V. Hill's Case: Periodic Orbits and Their Stability," *Astronomy and Astrophysics*, Vol. 1, February 1969, pp. 223–238.

[22] J. S. Parker and M. W. Lo, "Unstable Resonant Orbits near Earth and Their Applications in Planetary Missions," *AIAA/AAS Astrodynamics Specialist Conference*, Providence, Rhode Island, August 2004. AIAA 2004-22819.

[23] J. Demeyer and P. Gurfil, "Transfer to Distant Retrograde Orbits Using Manifold Theory," *Journal of Guidance, Control and Dynamics*, Vol. 30, September-October 2007, pp. 1261–1267.